Gundagani *et al.*
Journal of Engineering and Applied Science (2024) 71:9
https://doi.org/10.1186/s44147-023-00347-w

Journal of Engineering and Applied Science

RESEARCH Open Access

Finite element solutions of Double diffusion effects on three-dimensional MHD Nano-Powell-Erying fluid flow in presence of thermal and mass Biot numbers

Murali Gundagani[1*], Lakshmi Prasanna Mamidi[2] and Poorna Kantha Tanuku[3]

*Correspondence:
murali.maths81@gmail.com

[1] Department of Mathematics, Geethanjali College of Engineering and Technology, Cheeryal, India
[2] Department of Applied Mathematics, Andhra University, Visakhapatnam, India
[3] Department of Mathematics, GVP College of Engineering for Women, Visakhapatnam, India

Abstract

This work uses a numerical method to investigate the effects of diffusion on the flow of three-dimensional magnetohydrodynamic (MHD) nanofluids. The applicable equations for this problem are derived from the Nano-Powell-Erying fluid model. The result of the differential equation is calculated by solving the problem using the finite element method. The numerical solutions are used to study the three-dimensional structures with the flow of nanofluid to investigate the influence of well-known fluid parameters. The study found that the Hartmann number and buoyancy ratio parameter have a significant impact on the velocity profile, while the Brownian motion and thermophoresis parameters, as well as the thermal and mass Biot numbers, are the main factors influencing the temperature and concentration fields. This study aims to analyse the effect of two different parameters on the flow of MHD nanofluids to improve our basic understanding of this phenomenon. The findings that were produced are compared to the previous work and incipiently, the present numerical results are veritably in good agreement with the previous results. The results of this study can be useful for the optimization and design of various engineering applications.

Keywords: Three dimensional, Powell-Erying fluid, Nanofluid, Magnetic field, Porous medium, Thermal Biot number, Mass Biot number, Finite element method

Introduction

Nanofluids are a special sort of fluid that has nanoparticles floating throughout their whole. It is possible that the addition of nanoparticles may enhance the thermal and transport properties of the base fluid. As a result, the base fluid may become more desirable for use in cooling systems, heat exchangers, and lubricating systems. When a nanofluid is subjected to a temperature gradient, the Soret and Dufour effects that it exhibits may be analogous to those that have been seen in conventional fluids. The Soret effect is the tendency of a fluid to separate into its components when there is a temperature gradient, while the Dufour effect is the tendency of a fluid to mix its constituents when there is a concentration gradient. These affects have the potential to have a major effect

on the nanofluid's thermal and transport properties. It is essential to do research on the flow of nanofluids when the Soret and Dufour effects are present in order to have a comprehensive understanding of the behavior of nanoscale fluids in a variety of contexts. Models, both theoretical and numerical, are used extensively in the research that is done on these intricate processes of fluid dynamics and heat transfer.

The Powell-Erying fluid is a non-Newtonian fluid that exhibits shear-thinning behaviour. This implies that the Powell-Erying fluid's viscosity decreases as the shear rate rises. This fluid is put to work in a wide range of manufacturing processes, such as those involving the production of polymers and foods, as well as in drilling fluids for the oil and gas industry. When a Powell-Erying fluid is subjected to a temperature gradient, it is possible for the Soret and Dufour phenomena to take place. These natural occurrences are essential to the operation of a wide variety of commercial operations, including crystallization, thermal diffusion in gases, and geothermal energy systems. In the fields of fluid mechanics and heat transfer, there is a substantial amount of interest in the examination of the Powell-Erying fluid flow when the Soret and Dufour effects are present. The design and improvement of a great number of manufacturing processes might be facilitated by gaining an understanding of the behaviour of this kind of fluid under a variety of conditions. Researchers Kuznetsov and Nield [1] investigated the flow of a nanofluid's spontaneous convective boundary layer as it traversed a vertical plate. Kuznetsov and Nield [2] looked at the Soret and Dufour effects on heat and mass transfer in a porous medium that was saturated with a nanofluid. In their study, Chamkha and Al-Mudhaf [3] investigated the impact of Soret and Dufour on mixed convection emanating from a vertical surface in a nanofluid. The natural convection heat transfer of a nanofluid in a vertical cylindrical annulus with Soret and Dufour effects was investigated by Esfahani and Doostani [4]. Analytical solutions for the Soret and Dufour effects on natural convection were developed by Jafaryar and Hatami [5] in a vertical porous cavity that was filled with a nanofluid. Natural convection was investigated by Mohebbi, Hatami, and Rashidi [6], who took into account the Soret and Dufour effects throughout their research. The cavity in which their study was conducted was slanted and filled with a nanofluid. When investigating the unsteady magnetohydrodynamic (MHD) free convection flow of a nanofluid over an inclined plate with a radiation and heat source, Pal and Mondal [7] took into mind the Soret and Dufour effects. The Soret and Dufour effects were studied by Mahdy and Chamkha [8] in the natural convection of a nanofluid-filled container with active walls. The consequences of Soret and Dufour's work on the natural convection of a nanofluid in a porous cavity with sinusoidal temperature changes were investigated by Rahimi-Gorji and Hatami [9]. A summary of double-diffusive natural convection in nanofluids was provided in the review article [10] written by Manca and Nardini. Rashidi and Lorenzini [11] investigated how the effects of Soret and Dufour on MHD natural convection were manifested in a square cavity that was filled with a nanofluid. Soret and Dufour's impact on the natural convection of a nanofluid was studied by Saffari et al. [12] in a triangular enclosure with a sinusoidal temperature distribution on the bottom wall. Hajmohammad and Aminossadati [13] examined the Soret and Dufour effects on the natural convection of a nanofluid in a porous cavity using the lattice Boltzmann technique. In a lid-driven cavity, Jalilpour et al. [14] studied the Soret and Dufour effects on Al_2O_3-water nanofluid mixed convection heat transfer. Using the Soret and

Dufour effects, Marafie et al. [15] examined the transfer of heat and mass in nanofluids between stretched sheets. Samet and Abbasian Arani [16] explored the combined effects of Soret and Dufour on the flow and heat transmission of nanofluids through a variable-thickness stretched sheet. This was done in order to find out how these factors affect the flow and transmission of heat. The influence of Soret and Dufour on the MHD flow of nanofluid over a vertical plate subjected to a convective boundary condition was the subject of research conducted by Kumar and Singh [17].

Javed et al. [18] conducted a computational study to analyse the flow of Powell-Erying nanofluid in three dimensions, taking into account the impacts of Soret and Dufour. The modeling of Powell-Erying nanofluid double diffusion effects with heat generation/absorption was examined by Khan et al. [19]. Makinde et al. [20] investigated an unstable Powell-Erying nanofluid MHD flow while taking into account the impacts of Soret and Dufour. The effects of the Soret and Dufour equations on the MHD Powell-Eyring fluid flow over a convectively heated stretched sheet were studied by Motsa et al. [21]. Bég and Rashidi [22] conducted research on the peristaltic transport of a Powell-Eyring fluid over an asymmetric channel while taking into consideration the work of Soret and Dufour. The consequences of Soret and Dufour's work on the MHD Powell-Eyring fluid flow through a stretched sheet were studied by Das and Sahoo [23]. The synergistic impact of Soret and Dufour's contributions to magnetohydrodynamics Mustafa et al. [24] investigated Powell-Eyring fluid flow with heat transfer as part of their research. The influence of Soret and Dufour on the heat and mass transfer of Powell-Eyring fluid via a stretched sheet was explored by Sulochana and Vijaya Kumar [25]. Alam et al. [26] conducted an investigation on the impact that Soret and Dufour have on the unstable Powell-Eyring fluid flow that occurs over a stretched sheet. The MHD Powell-Eyring fluid flow across a stretched sheet was studied by Partha and colleagues [27] who took into account the Soret and Dufour effects. Researchers Hayat et al. [28] investigated the effects of heat radiation and chemical reaction on the MHD flow of Powell-Eyring fluid. Computational research was conducted by Ramzan et al. [29] to investigate the heat and mass transport parameters of the Powell-Eyring fluid model when applied to a stretched sheet with nonlinear thermal radiation, the Soret effect, and the Dufour effect. Khalid et al. [30] looked at the impact that thermal radiation and convective circumstances have on the Powell-Eyring fluid model with the Dufour and Soret effects. Khan et al. [31] used the Soret and Dufour effects in their investigation of the non-linear radiative flow of Powell-Eyring fluid through a stretched cylinder. A computer investigation of the Powell-Eyring fluid with Soret and Dufour effects over a nonlinear stretching sheet is performed by Khan et al. [32]. The numerical investigation of Powell-Eyring fluid flow with Dufour and Soret effects was carried out by Raja et al. [33]. Saqib and Alsaedi [34] explored heat and mass transmission in a Powell-Eyring fluid model with Soret and Dufour effects over a stretched surface. Gundagani et al. [35] investigated the effects of radiation on an unsteady MHD convective flow past a semi-infinite vertical permeable moving plate embedded in a porous medium with viscous dissipation. Gadipally et al. [36] investigated the soret and dufour effects on unsteady MHD flow past a semi-infinite vertical porous plate. Using the finite element method, Gundagani et al. [37] discovered the solution for the thermal radiation effect on unsteady MHD flow past a vertical porous plate with variable suction. Murali et al. [38] analyzed heat and mass transfer

effects on an unsteady hydromagnetic free convective flow over an infinite vertical plate embedded in a porous medium with heat absorption. The Soret and Dufour effects on unsteady hydromagnetic free convective fluid flow past an infinite vertical porous plate in the presence of chemical reaction were investigated by Babu et al. [39]. The above cited works had a significant impact on understanding the nature of the reported work.

The preceding investigation, which was prompted by the aforementioned reference works, demonstrates that the joint effects of thermal and mass Biot numbers on three-dimensional, steady, viscous, incompressible, electrically conducting Powell-Erying fluid flow towards an exponentially stretching sheet filled with porous medium in the presence of Thermophoresis, Soret, Brownian motion, and Dufour effects can be determined through the application of numerical solutions. In this piece of research, a mathematical model known as the Eyring-Powell is constructed and then solved with the use of the finite element method. Plots and numerical data are used to verify the convergence of computed solutions.

Methods

In this section, we consider an incompressible, thick, steady, three-dimensional MHD inflow of electrical conducting Powell-Eyring-nanofluid over an exponential stretching distance filled by pervious medium in the presence of thermal prolixity, prolixity thermo, thermal Biot number, and mass Biot number. Figure 1 depicts the physical match system and figure of this problem for this inflow. For this disquisition, the following hypotheticals are made of the following:

i. Assuming that an invariant transverse magnetic field of strength Bo is applied resembling to the *z*-axis.

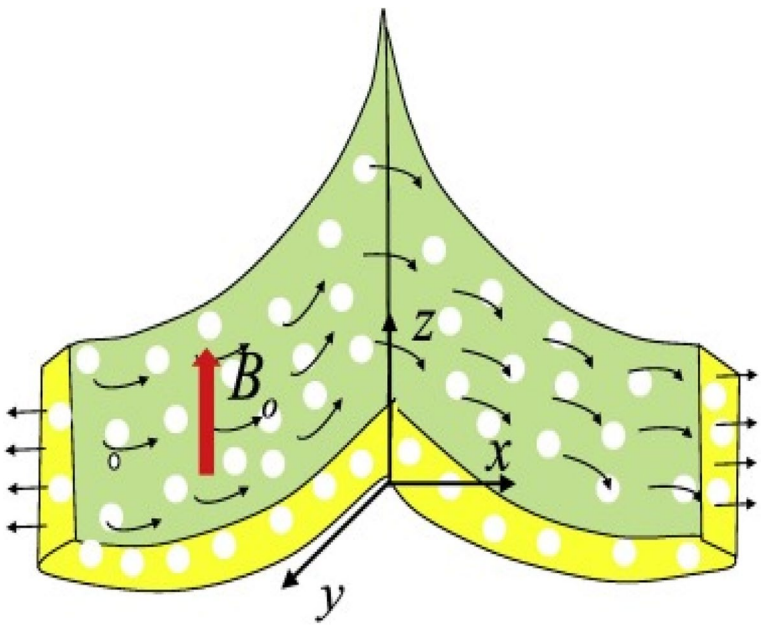

Fig. 1 Geometrical design of Nano-Powell-Erying fluid flow

ii. As Reynolds number has considered as small. So, convinced glamorous and electric field are neglected.
iii. The goods of heat source, joule heating, and thick dispersion are neglected.
iv. The effect of chemical response is neglected in attention equation. Convective boundary condition is employed where the face of the distance gets heated by a hot fluid of invariant temperature Tf, attention Cf, the convective heat transfer measure β1, and mass transfer measure λ1.

Grounded on the below hypothetical's, the introductory equations for this inflow, the governing boundary equations can be written as follows:

Continuity equation

$$\frac{\partial u}{\partial x}+\frac{\partial v}{\partial y}+\frac{\partial w}{\partial z}=0 \tag{1}$$

Momentum equation

$$u\left(\frac{\partial u}{\partial x}\right)+v\left(\frac{\partial u}{\partial y}\right)+w\left(\frac{\partial u}{\partial z}\right)=\left(v+\frac{1}{\rho\chi C^{*}}\right)\left(\frac{\partial^{2}u}{\partial z^{2}}\right)-\frac{1}{2\rho\chi C^{*3}}\left(\frac{\partial u}{\partial z}\right)^{2}\left(\frac{\partial^{2}u}{\partial z^{2}}\right)-\left(\frac{v}{k^{*}}\right)u-\left(\frac{\sigma B_{0}^{2}}{\rho}\right)u \tag{2}$$

$$u\left(\frac{\partial v}{\partial x}\right)+v\left(\frac{\partial v}{\partial y}\right)+w\left(\frac{\partial v}{\partial z}\right)=\left(v+\frac{1}{\rho\chi C^{*}}\right)\left(\frac{\partial^{2}v}{\partial z^{2}}\right)-\frac{1}{2\rho\chi C^{*3}}\left(\frac{\partial v}{\partial z}\right)^{2}\left(\frac{\partial^{2}v}{\partial z^{2}}\right)-\left(\frac{v}{k^{*}}\right)v-\left(\frac{\sigma B_{0}^{2}}{\rho}\right)v \tag{3}$$

Equation of thermal energy

$$u\left(\frac{\partial T}{\partial x}\right)+v\left(\frac{\partial T}{\partial y}\right)+w\left(\frac{\partial T}{\partial z}\right)=\alpha_{m}\left(\frac{\partial^{2}T}{\partial z^{2}}\right)+\tau_{B}\left\{\left\{D_{B}\left(\frac{\partial T}{\partial z}\right)\left(\frac{\partial C}{\partial z}\right)+\frac{D_{T}}{T_{\infty}}\left(\frac{\partial T}{\partial z}\right)^{2}\right\}+\frac{D_{m}K_{T}}{C_{s}C_{p}}\left(\frac{\partial^{2}C}{\partial z^{2}}\right)\right. \tag{4}$$

Equation of species concentration

$$u\left(\frac{\partial C}{\partial x}\right)+v\left(\frac{\partial C}{\partial y}\right)+w\left(\frac{\partial C}{\partial z}\right)=D_{B}\left(\frac{\partial^{2}C}{\partial z^{2}}\right)+\frac{D_{T}}{T_{\infty}}\left(\frac{\partial T}{\partial z}\right)^{2}\frac{D_{m}K_{T}}{T_{m}}\left(\frac{\partial^{2}C}{\partial y^{2}}\right) \tag{5}$$

where $\tau_{B}=\left(\frac{(\rho C)_{\rho}}{(\rho C)_{f}}\right)$.

The boundary conditions for this flow are as follows:

$$\left.\begin{array}{c} u=u_{w}=U_{o}\exp\left(\frac{x+y}{L}\right),v=v_{w}=V_{o}\exp\left(\frac{x+y}{L}\right), \\ -K\frac{\partial T}{\partial z}=\beta_{1}\left(T_{f}-T\right),-D_{B}\frac{\partial C}{\partial z}=\lambda_{1}\left(C_{f}-C\right) \end{array}\right\}atz=0 \\ u\to 0,v\to 0,T\to T_{\infty},C\to C_{\infty}asz\to\infty \Bigg\} \tag{6}$$

Introducing the following similarity transformations

$$\left.\begin{array}{c} u=U_{o}\exp\left(\frac{x+y}{L}\right)f\prime(\eta),v=V_{o}\exp\left(\frac{x+y}{L}\right)\mathrm{g}\prime(\eta),\theta=\frac{T-T_{\infty}}{T_{f}-T_{\infty}},\varnothing=\frac{C-C_{\infty}}{C_{f}-C_{\infty}} \\ w=-\sqrt{\frac{vU_{o}}{2L}}\exp\left\{\frac{(x+y)}{2L}\right\}\left\{f(\eta)+\eta f^{\prime(\eta)}+\mathrm{g}(\eta)+\eta\mathrm{g}^{\prime(\eta)}\right\},\eta=\left(\sqrt{\frac{U_{0}}{2vL}}\right)\exp\left\{\frac{(x+y)}{2L}\right\}z, \end{array}\right\} \tag{7}$$

Making use of Eq. (7), equation of continuity (1) is identically satisfied and Eqs. (2), (3), (4), and (5) take the following form:

$$(1+\beta)f^{\prime\prime\prime}-\beta\lambda f^{\prime\prime\prime}f^{\prime\prime 2}+ff^{\prime\prime}+\mathrm{g}f^{\prime\prime}-2f^{\prime 2}-2\mathrm{g}f^{\prime}-(M+K)f^{\prime}=0 \tag{8}$$

$$(1+\beta)\mathrm{g}''' - \beta\lambda \mathrm{g}'''\mathrm{g}'^2 + f\mathrm{g}'' + \mathrm{g}\mathrm{g}'' - 2\mathrm{g}'^2 - 2f\mathrm{g}' - (M+K)\mathrm{g}' = 0 \tag{9}$$

$$\theta'' + \mathrm{Pr} f\theta\prime + \mathrm{Prg}\theta\prime + \mathrm{Pr}Nb\theta\prime\phi\prime + \mathrm{Pr}Nt\theta'^2 + \mathrm{Pr}Du\phi\prime\prime = 0 \tag{10}$$

$$Nb\phi'' + NbScf\phi\prime + NbScg\phi\prime + Nt\theta'' + ScNbSr\theta'' = 0 \tag{11}$$

The corresponding boundary conditions (6) becomes the following:

$$\left.\begin{array}{c} f(0)=0, \mathrm{g}(0)=0, f'(0)=1, \mathrm{g}'(0)=, \theta'(0)=-\delta(1-\theta(0)), \phi'(0)=-(1-\phi(0)) \\ f\prime(\infty)\to 0, \mathrm{g}\prime(\infty)\to 0, \theta(\infty)\to 0, \phi(\infty)\to 0 \end{array}\right\} \tag{12}$$

where the involved physical parameters are defined as follows:

$$\left.\begin{array}{c} M=\frac{2\sigma B_o^2 L}{\rho U_o}, K=\frac{2\nu L}{k^* U_o}, =\frac{V_o}{U_o}, Nb=\frac{\tau_B D_B\left(C_f-C_\infty\right)}{\nu}, \mathrm{Pr}=\frac{\nu}{\alpha_m}, \\ \beta=\frac{1}{\mu\chi C^*}, \lambda=\frac{u_w^3}{2\nu x C^{*2}}, Nt=\frac{\tau_B D_T\left(T_f-T_\infty\right)}{\nu T_\infty}, Sr=\frac{D_m K_T\left(T_f-T_\infty\right)}{T_m\nu\left(C_f-C_\infty\right)}, \\ Du=\frac{D_m K_T\left(C_f-C_\infty\right)}{C_s C_p\nu\left(T_f-T_\infty\right)}, \delta\frac{\beta_1}{K}\sqrt{\frac{2L\nu}{U_o}}, =\frac{\lambda_1}{D_B}\sqrt{\frac{2L\nu}{U_o}}, Sc=\frac{\nu}{D_B}, \end{array}\right\} \tag{13}$$

Quantities of physical interest, the physical parameters of the skin-friction coefficient along x- and y-directions, and local Nusselt and Sherwood numbers are presented as follows:

$$Cf_x = \frac{2\tau_{wx}}{\rho U_o^2} \Rightarrow Cf_x\left(\sqrt{\frac{Re_x}{2}}\right) = \left\{(1+\beta)f\prime\prime(0) - \frac{1}{3}\beta\lambda f\prime^3(0)\right\} \tag{14}$$

$$Cf_y = \frac{2\tau_{wy}}{\rho V_o^2} \Rightarrow \left(\sqrt{\frac{Re_y}{2}}\right)Cf_y = \left\{(1+\beta)\mathrm{g}\prime\prime(0) - \frac{1}{3}\beta\lambda \mathrm{g}\prime^3(0)\right\} \tag{15}$$

$$Nu_x = \frac{xq_w}{K\left(T_f - T_\infty\right)} = -\frac{x\left(\frac{\partial T}{\partial z}\right)_{z=0}}{K\left(T_f - T_\infty\right)} \Rightarrow \left(\sqrt{\frac{2}{Re_x}}\right)Nu_x = -\frac{x}{L}\theta\prime(0) \tag{16}$$

$$Sh_x = \frac{xq_m}{D_B\left(C_f - C_\infty\right)} = -\frac{x\left(\frac{\partial C}{\partial y}\right)_{y=0}}{D_B\left(C_f - C_\infty\right)} \Rightarrow \left(\sqrt{\frac{2}{Re_x}}\right)Sh_x = -\frac{x}{L}\phi\prime(0) \tag{17}$$

where $\mathrm{Re}_x = \frac{U_o x}{\nu}$ is the local Reynolds number based on the stretching velocity $u_w(x)$ and $\mathrm{Re}_y = \frac{V_o y}{\nu}$ is the local Reynolds number based on the stretching velocity $v_w(y)$.

Solution by FEM

The idea that the problem domain can be segmented into smaller, more manageable chunks that also have limited dimensions and are referred to as "finite elements" is the driving force behind the finite element approach. This idea was inspired by the fact that these chunks can be broken down into smaller, more manageable chunks. It has been put to use in the attempt to provide an explanation for a broad variety of occurrences, including as the transmission of heat, the mechanics of fluids and solids, the dynamics of

rigid bodies, the mechanics of solids, chemical processes, electrical systems, and acoustics. The use of the finite element approach is shown in (Fig. 2), which also serves as an example. Before you may go on to doing a finite element analysis, you are required to finish the phases that are listed below, which are as follows:

- Domain discretization into elements

As part of the finite element discretization process, the whole interval is segmented into a limited number of even smaller intervals, each of which is referred to as an element. These elements are then broken down into even smaller intervals.

- Elementation of the domain

After the domain has been elementalized, and each of the elements that were mentioned before may be found in the finite-element mesh.

In order to formulate equations for elements, please make use of the techniques that are supplied down below.

a) Use of the standard problem gets under way at a fairly early level in the iterative procedure of the mathematical version
b) While the variational problem has an approximation of the answer, the detailed equations are generated by substituting the approximation of the solution into a device that was constructed earlier, which is then solved for the variable.

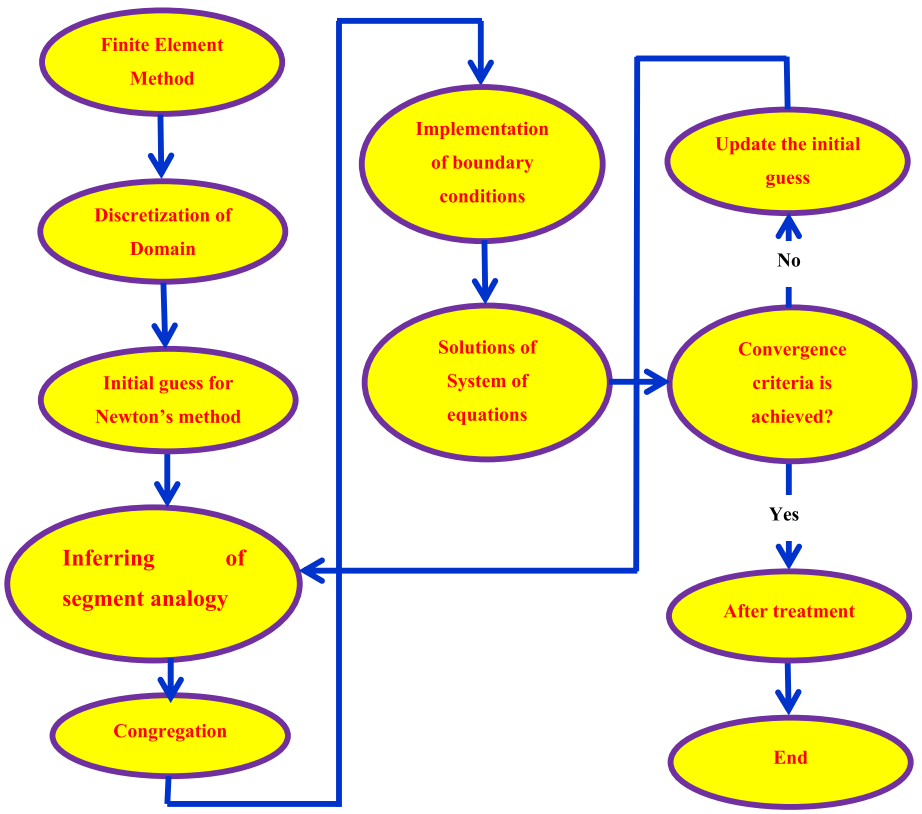

Fig. 2 Schema chart of FEM

c) The element equations can also be generated by solving the variational problem directly. This procedure is carried out many times until the equations for the elements have been formulated. This procedure is repeated until each and every variable has been uncovered, and then, it moves on to the next step.
d) The construction of the stiffness matrix made extensive use of a polynomial interpolation matrix as the primary instrument.
e) Constructing equations and determining the answers to those equations:

Every single algebraic equation has to be constructed by putting inter element continuity limits on each of the component parts of each equation. This is a necessary step in the construction of every single equation. Putting together an algebraic equation can only be done in this manner. This stage has to be finished before moving on to the next one, which is trying to solve the equations. It is necessary to incorporate an extremely large number of algebraic equations into a single set of equations in order to be able to create a global finite-element model of the whole domain.

- Imposing boundary conditions

In order to carry out an accurate analysis of the flow model, the boundary conditions need to be imposed on the equations that have already been formed into the model. This is necessary so that the conditions may be applied to the boundaries of the model.

The resolution of generated equations may be accomplished by the use of a wide variety of numerical techniques, including the LU decomposition method, the Gauss elimination method, and a great deal more besides. The solution of built equations is one of the most popular uses for these approaches. When working with real numbers, it is very necessary to bear in mind the form functions that are used to make an approximate approximation of real functions. Form functions may be used to provide a close approximation of real functions. If you follow this technique step by step, you may be certain that your calculations will be accurate. The flow domain has a total of 20,001 nodes and is divided into 10,000 quadratic components that are all the same size. These components are all of the same shape. The flow domain is made up of 10,000 quadratic components, all of which are of the same magnitude as their counterparts in the other components. After the element equations were developed, there were a total of 80,004 nonlinear equations that could be investigated. These equations were made accessible for study (Fig. 2).

After the boundary conditions have been applied, the Gauss approach is used to remove the remaining system of nonlinear equations, and then, the Gauss technique is used to arrive at a numerical solution that is accurate to 0.00001°. The use of gaussian quadrature is done so that the challenges that are connected to integration may be aided in some way.

The method's custom software was run on a desktop computer within the context of a suitable programming environment. The software was developed specifically for the method. MATHEMATICA is the name of the programming language that was used to create the software application for the computer.

Table 1 Comparison of present skin-friction coefficient along *x*- and *y*-direction results for $\vartheta = 0.1$ when $\beta = \lambda = M = Sr = Du = \zeta = 0$

M	Present skin-friction coefficient results along *x*-direction	Nadeem et al. [40] results	Present skin-friction coefficient results along *y*-direction	Nadeem et al. [40] results
0.0	1.15968817396873980	1.1648	2.5778692813983450	2.5874
10.0	3.36477819871698120	3.3767	4.3667891983749340	4.3787
100.0	10.0678659819833452	10.0763	12.068678291983925	12.0763

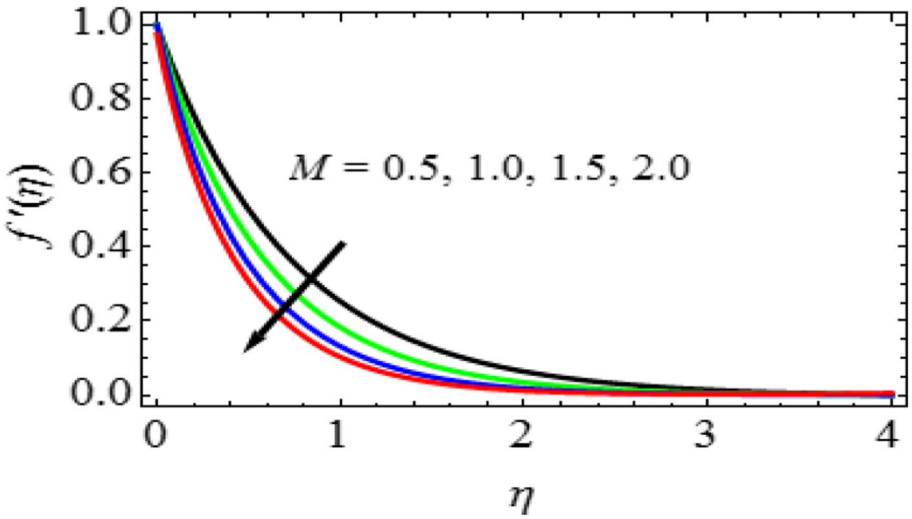

Fig. 3 *M* characteristics on $f'(\eta)$

Program code validation

For program code validation, the present results are compared to and validated against the available data in the literature provided by Nadeem et al. [40] in Table 1 and numerical results are found to be in excellent agreement, demonstrating the accuracy.

Results and discussion

Graphical data has been collected on sluice inflow haste, temperature, and attention biographies against colourful parameters. Figures 3 and 4 demonstrate the variations of glamorous field parameter on primary and haste biographies. As M elevates, a resistive force analogous to a drag force is generated, which is known as Lorentz force. Both the haste biographies are broken by the Lorentz force, which decelerates its stir. Figures 5 and 6 illustrate the goods of permeability parameter on the primary and secondary haste biographies. It is concluded from these numbers that the haste biographies are diminishments with the increased in the porosity parameter K. This happens due to the fact that an increase in K amplifies the pervious subcaste and hence reduces the consistence of instigation boundary sub caste. Figures 7 and 8 explore the fluid variable β impact on primary and secondary haste biographies.

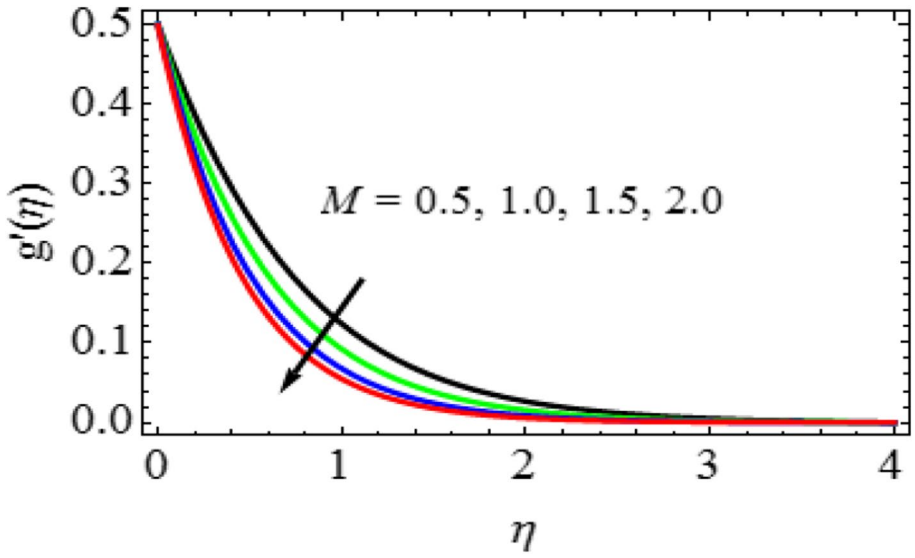

Fig. 4 *M* characteristics on $g^{'}(\eta)$

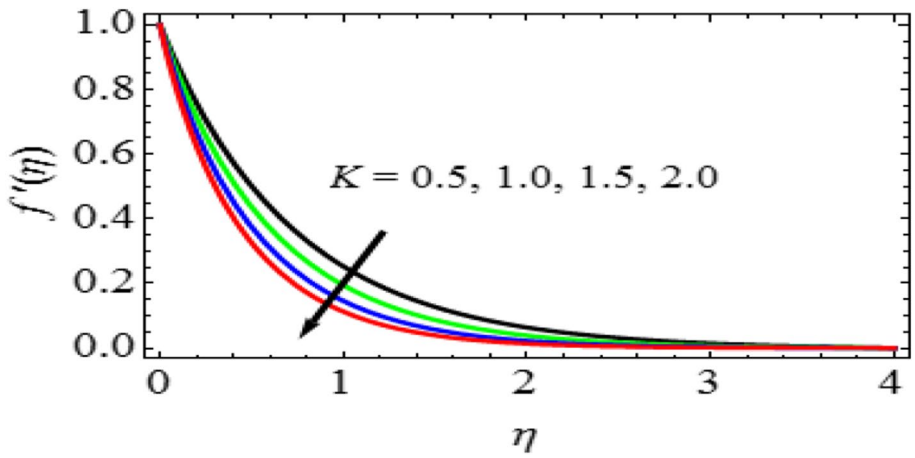

Fig. 5 *K* characteristics on $f^{'}(\eta)$

We can see both the haste biographies and the boundary subcaste consistence are enhanced via larger β. Physically, advanced values of beget the density to drop, performing in increased fluid haste. Figures 9 and 10 explain the characteristics of primary and secondary haste biographies are dwindling geste for larger λ. Figure 11 shows the geste of haste portion parameter on secondary haste biographies. From this figure, it is observed that the secondary haste biographies are adding with rising values of haste rate parameter.

The Fig. 12 shows how the Prandtl number affects the temperature field. Brownian stir parameter (Nb) consequences for temperature and attention biographies sequentially are shown in Figs. 13 and 14. In Fig. 13, the temperature biographies are enhanced when the Brownian stir parameter Nb is increased. From Fig. 14, it is observed that attention

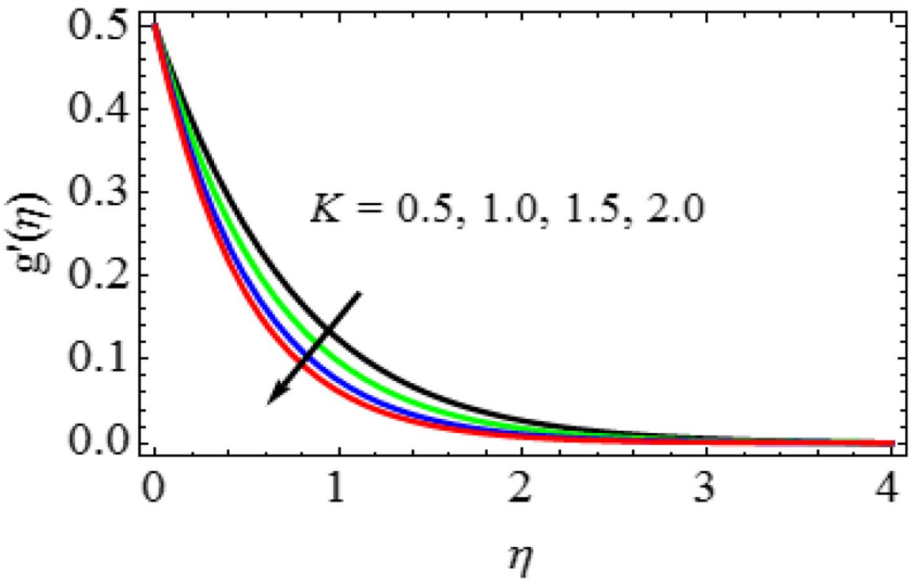

Fig. 6 *K* characteristics on $g'(\eta)$

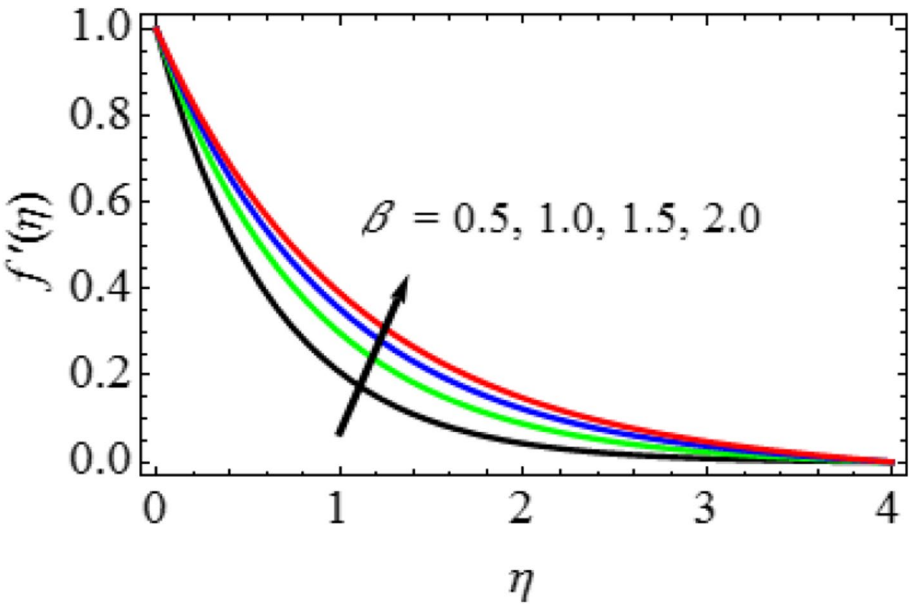

Fig. 7 β characteristics on $f'(\eta)$

decreases with the proliferation of Nb. The effect of thermophoresis parameter (Nt) on temperature and attention biographies are displayed in Figs. 15 and 16 independently. Thermophoresis parameter depends on thermal prolixity measure and thick force. Figures 17 and 18, one after the other, so that you can see how the Dufour number, and the Soret number, bear in relation to the temperature and attention biographies. When examining this figure, we set up that adding the value of Du led to a rise in both the

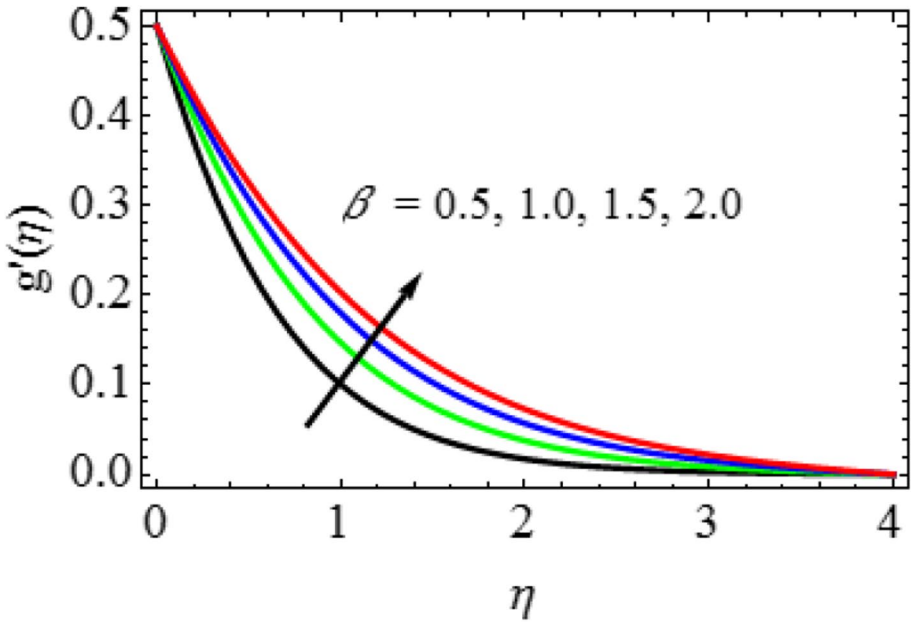

Fig. 8 β characteristics on $g'(\eta)$

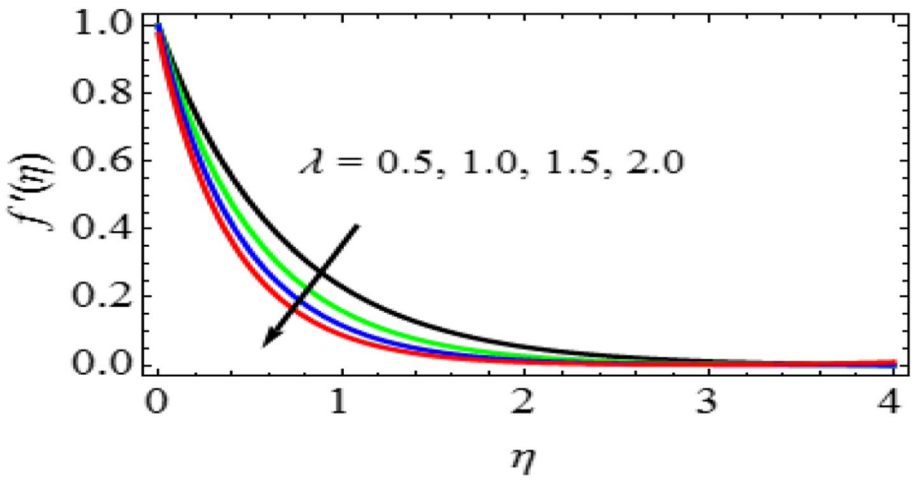

Fig. 9 λ characteristics on $f'(\eta)$

temperature and the consistence of the thermal subcaste. The impact of an attention grade on the thermal energy contained inside a liquid is physically related to Du. analogous to how adding Sr situations improves attention biographies, so do rising Sr values. This is due to the fact that a temperature grade facilitates the transfer of mass from a lower to a lesser attention of the solute. Figure 19 illustrates the influence of Schmidt number (Sc) on attention biographies. The Sc value is a representation of the rate of the instigation to the mass diffusivity. By using prolixity in the attention (species) boundary subcaste, it measures the relative value of instigation and mass transport. Advanced Sc

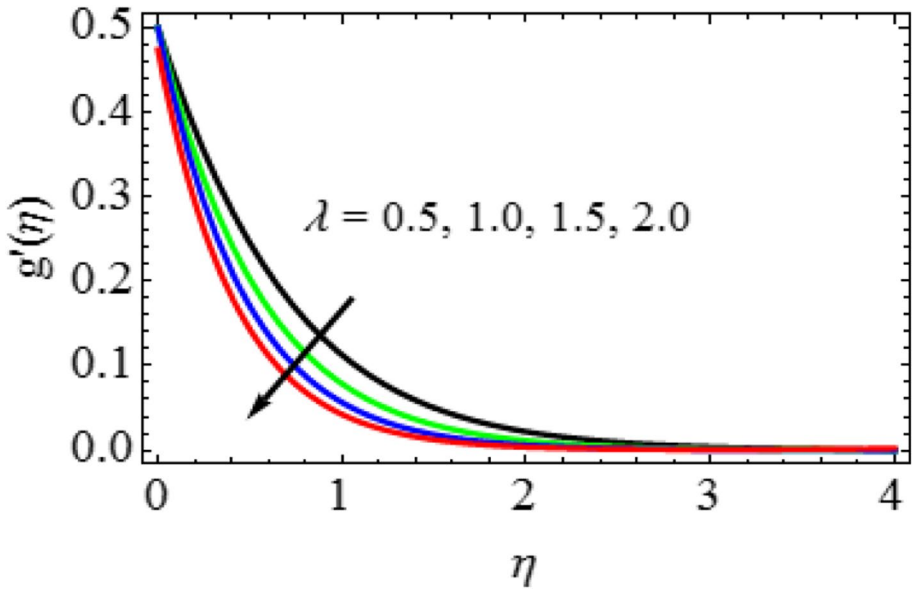

Fig. 10 λ characteristics on $g'(\eta)$

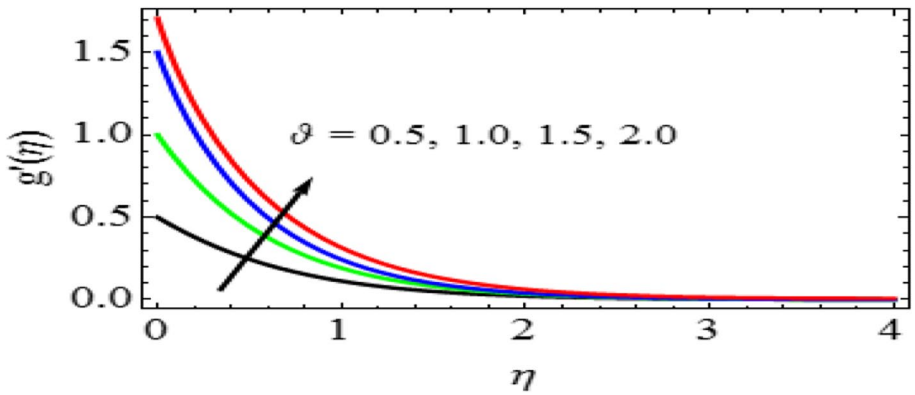

Fig. 11 ϑ characteristics on $g'(\eta)$

will lower the fluid's mass diffusivity, which will affect in lower attention biographies. Larger values of Sc actually correspond to weaker attention boundary layers because mass diffusivity and the Sc have an inverse. The consequence of the thermal Biot number on the temperature field can be observed in Fig. 20. A rise in δ induces the convection to be stronger, which amplifies the temperature field. An improvement in δ leads to a stronger convection which shows an improvement in the temperature field. Figure 21 illustrates the effect of mass Biot number on the attention biographies. Attention biographies are an adding function of mass Biot number. Tables 2 and 3 show the numerical values of the skin disunion portions in x- and y-directions for diversions in the values of the colorful parameters similar to M, K, β, λ, ϑ, Pr, Nt, Nb, Du, δ, Sc, Sr, ζ. From these tables, it is observed that the skin disunion portions in x and y directions are adding with

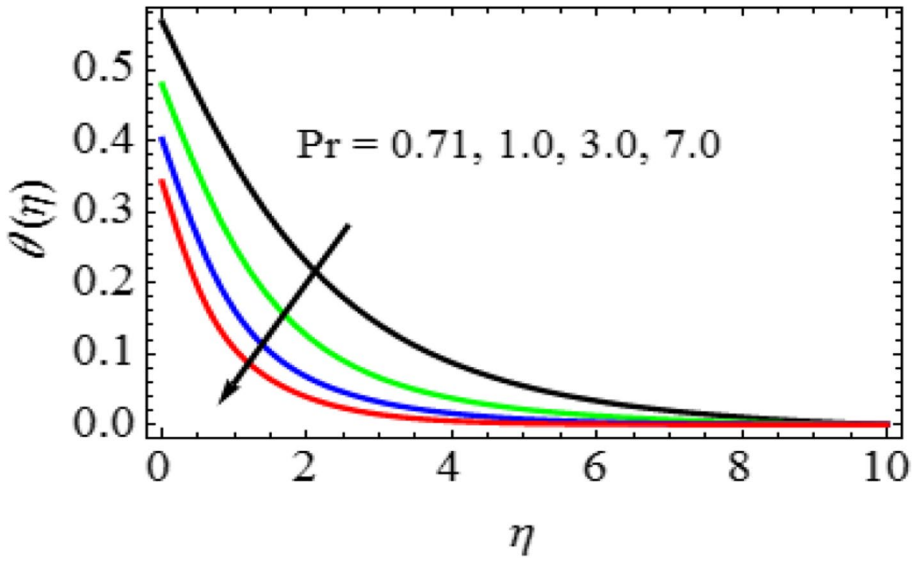

Fig. 12 Pr characteristics on $\theta(\eta)$

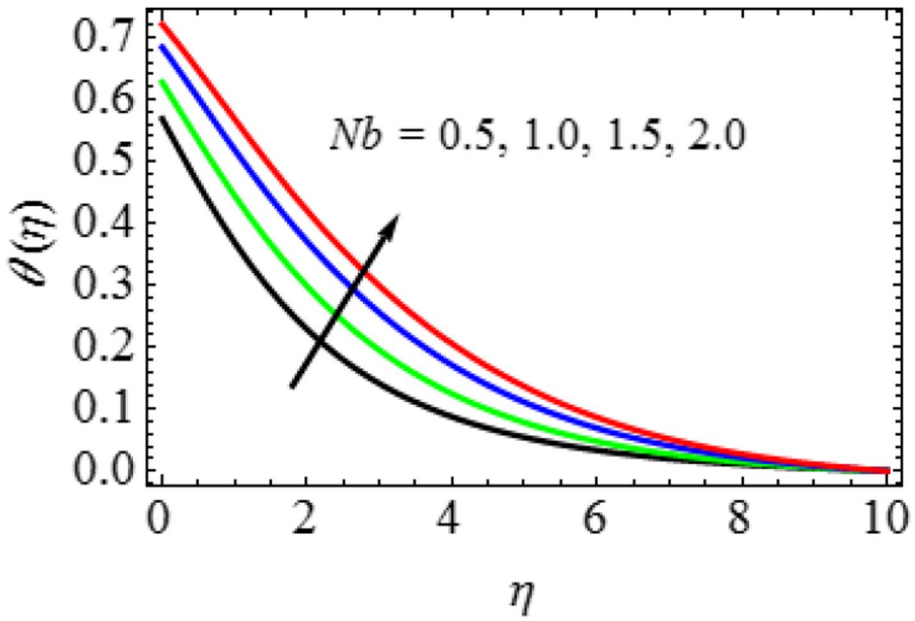

Fig. 13 *Nb* characteristics on $\theta(\eta)$

rising values of ϑ, Nt, Nb, Du, δ, Sr, and ζ, while its dwindling with adding values of M, K, β, λ, Pr, and Sc. Tables 4 and 5 are showing the numerical values of rate of heat transfer measure and mass transfer measure independently.

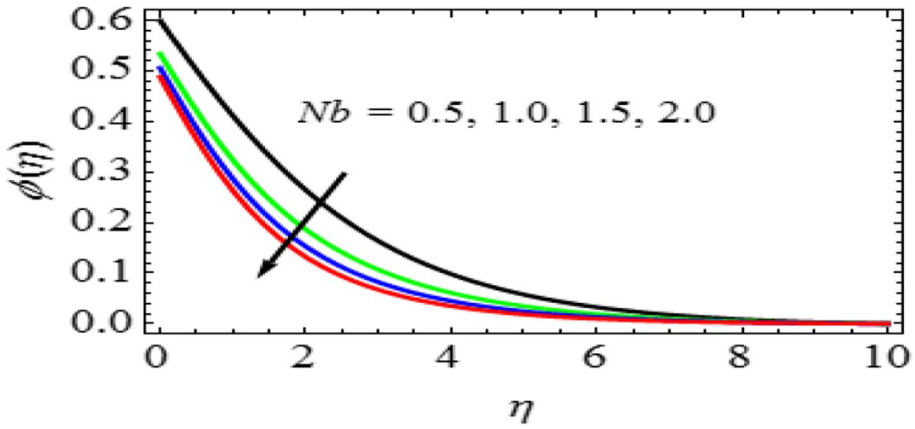

Fig. 14 *Nb* characteristics on φ (η)

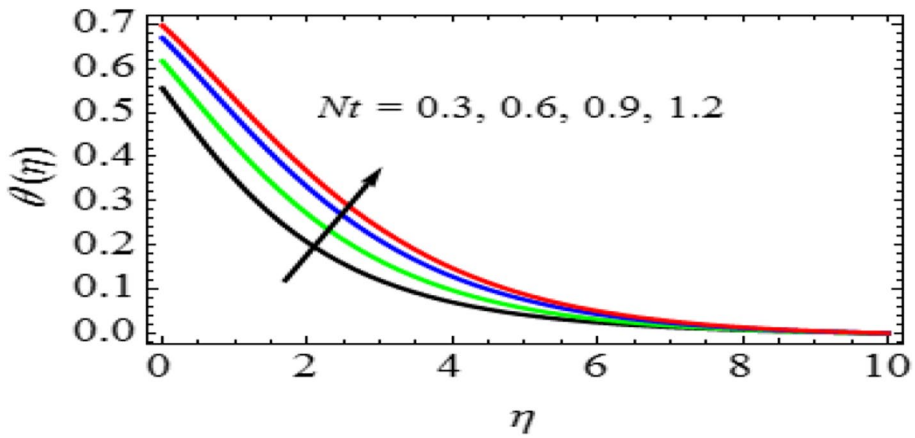

Fig. 15 *Nt* characteristics θ (η)

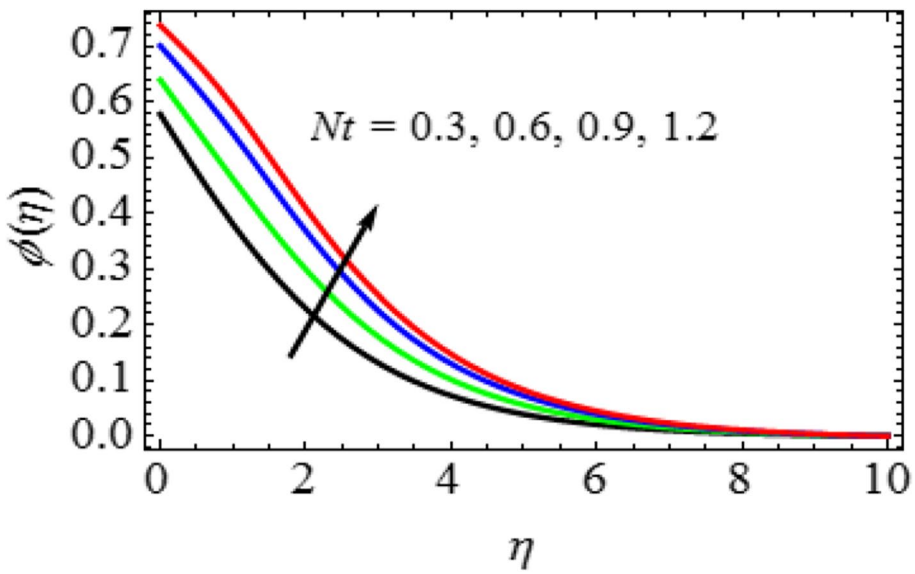

Fig. 16 *Nt* characteristics on φ (η)

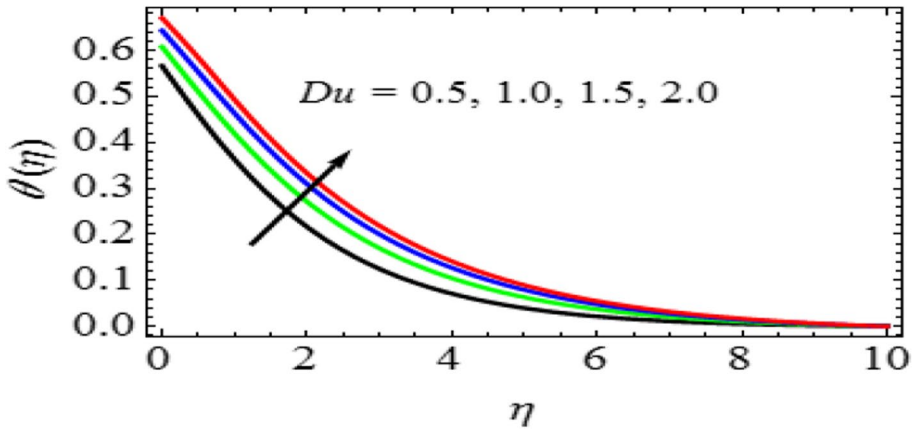

Fig. 17 *Du* characteristics on $\theta(\eta)$

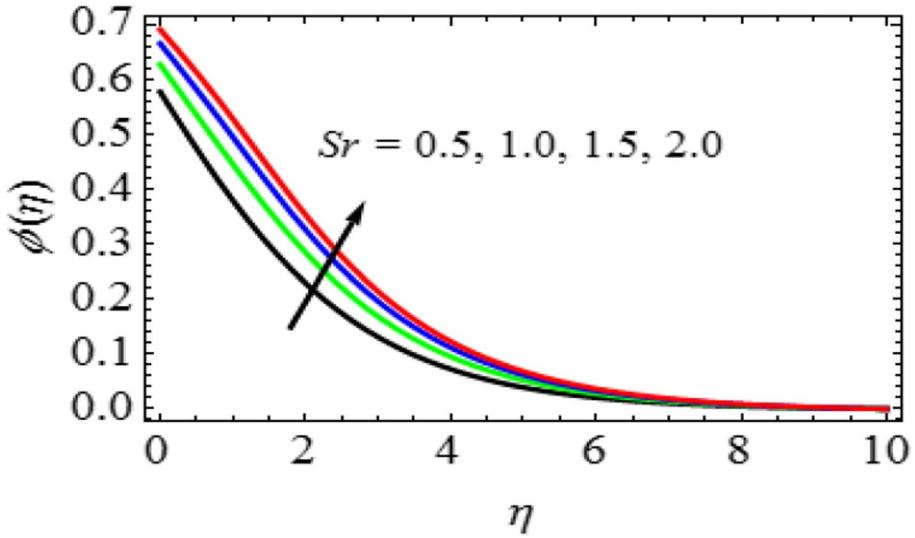

Fig. 18 *Sr* characteristics on $\varphi(\eta)$

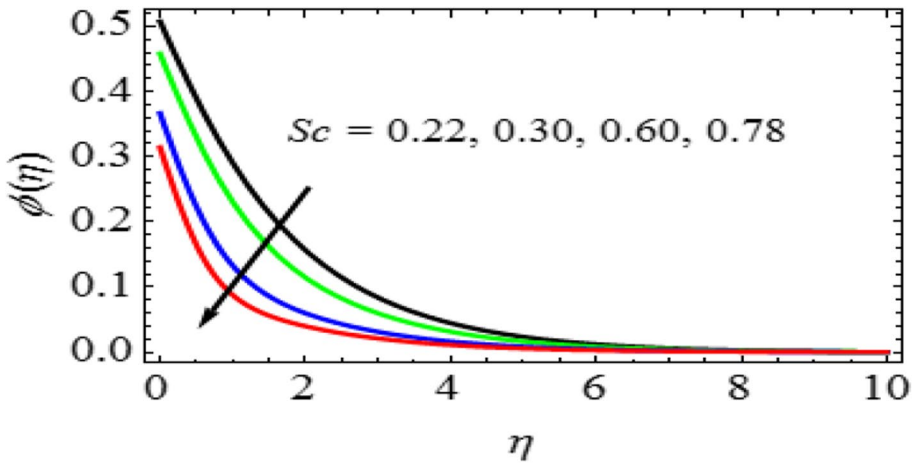

Fig. 19 *Sc* characteristics on $\varphi(\eta)$

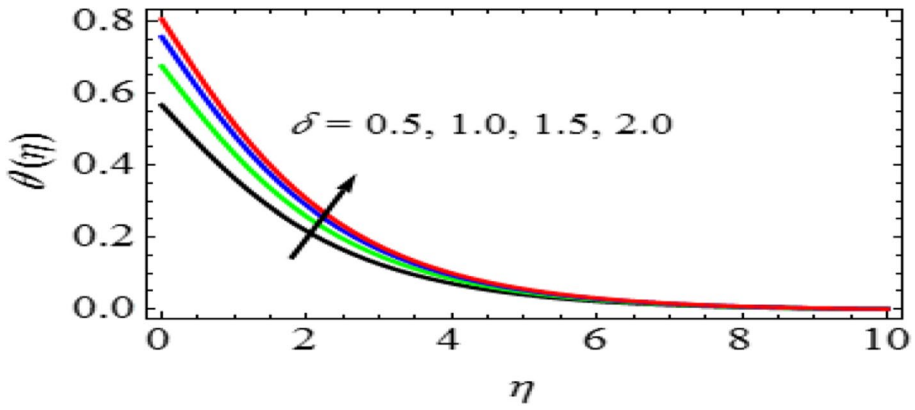

Fig. 20 δ characteristics on $\theta(\eta)$

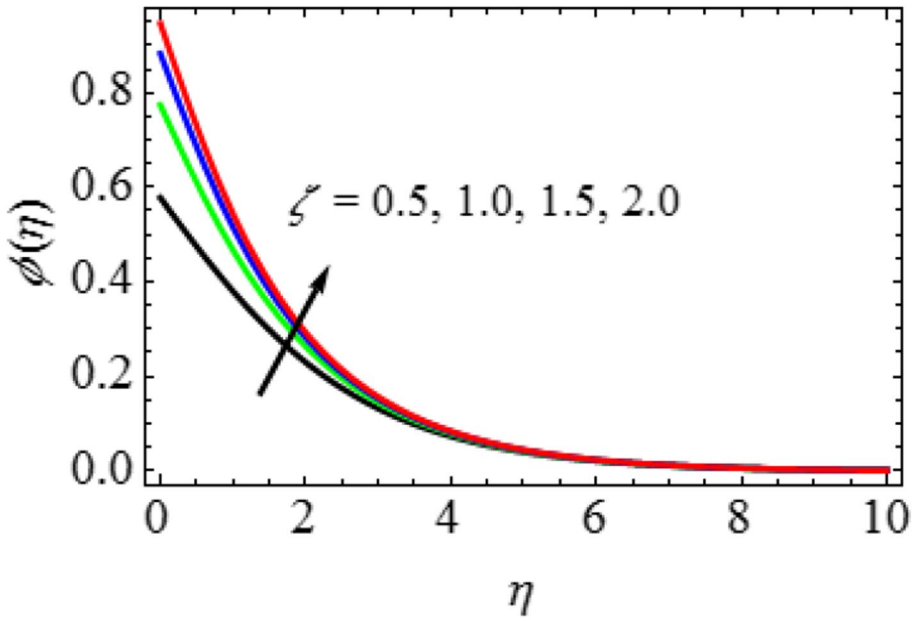

Fig. 21 ζ characteristics on $\varphi(\eta)$

Primary and secondary velocity profiles (Figs. 3, 4, 5, 6, 7, 8, 9, 10, and 11)

Temperature and concentration profiles (Figs. 12, 13, 14, 15, 16, 17, 18, 19, 20, and 21)

Conclusions

Extensive numerical parametric study is performed on the numerical solution of a class of nonlinear equations to describe the details of the solution and results are reported in terms of graphs. Effects of thermal Biot number, mass Biot number, Soret, and Dufour on Powell-Erying fluid towards an exponentially stretching sheet in the presence of magnetic field, nanofluid particles, porous medium, Brownian motion, and thermophoresis effects are analyzed. The numerical solutions are used to study

Table 2 Skin-friction coefficient along *x*-direction results

M	*K*	*β*	*λ*	*ϑ*	Pr	*Nt*	*Nb*	*Du*	*δ*	*Sc*	*Sr*	*ζ*	$f''(0)$
0.5	0.5	0.5	0.5	0.5	0.71	0.3	0.5	0.5	0.5	0.22	0.5	0.5	2.3567467850
1.0													2.3183761738
1.5													2.2967863933
	1.0												2.3285791867
	1.5												2.3009383988
		1.0											2.3297134703
		1.5											2.3064378946
			1.0										2.3198579134
			1.5										2.2998768798
				1.0									2.3778424004
				1.5									2.3967193789
					1.00								2.3112462447
					7.00								2.2878739841
						0.6							2.3856479989
						0.9							2.4146573378
							1.0						2.3777893483
							1.5						2.4013474552
								1.0					2.3914532805
								1.5					2.4196786793
									1.0				2.3735647968
									1.5				2.3878757591
										0.30			2.3115673402
										0.78			2.2978853860
											1.0		2.3667584523
											1.5		2.3856348772
												1.0	2.3696768984
												1.5	2.3873480650

the three-dimensional structures with the flow of nanofluid to investigate the influence of well-known fluid parameters. In some special cases for the validity and delicacy of the results have been attained from the current results. The findings that were produced are compared to the work that had been published in the history. The following are the main findings from this analysis.

- The primary and secondary velocity profiles are decreasing with increasing values of Powell-Erying fluid parameters, permeability parameter, and magnetic field parameter.
- The secondary velocity profiles are growing with rising values of velocity ratio parameter.
- The temperature profiles are increasing with increasing values of thermophoresis parameter, Brownian motion parameter, Dufour number, and thermal Biot number, whereas the Prandtl number has reduced the temperature profiles.

Table 3 Skin-friction coefficient along *y*-direction results

M	*K*	*β*	*λ*	ϑ	Pr	*Nt*	*Nb*	*Du*	*δ*	*Sc*	*Sr*	*ζ*	$g''(0)$
0.5	0.5	0.5	0.5	0.5	0.71	0.3	0.5	0.5	0.5	0.22	0.5	0.5	1.5767896303
1.0													1.5478384938
1.5													1.5267538749
	1.0												1.5577483896
	1.5												1.5398773687
		1.0											1.5246730346
		1.5											1.4976734734
			1.0										1.5546768349
			1.5										1.5367775831
				1.0									1.5967839198
				1.5									1.6196663796
					1.00								1.5498434678
					7.00								1.5214674822
						0.6							1.5906893981
						0.9							1.6226703676
							1.0						1.5846730942
							1.5						1.5911149694
								1.0					1.5916374634
								1.5					1.6287507633
									1.0				1.5896736946
									1.5				1.5996783409
										0.30			1.5625678680
										0.78			1.5498573874
											1.0		1.5815265965
											1.5		1.6025657340
												1.0	1.5815670794
												1.5	1.5947685731

Table 4 Rate of heat transfer coefficient results

Pr	*Nt*	*Nb*	*Du*	*δ*	Nu_x
0.71	0.3	0.5	0.5	0.5	0.8566473873
1.00					0.8267833939
7.00					0.8015673487
	0.6				0.8715674022
	0.9				0.8967476205
		1.0			0.8867589038
		1.5			0.9016734064
			1.0		0.8867383749
			1.5		0.9116594386
				1.0	0.8767348903
				1.5	0.8891673067

- The concentration profiles are decreasing with increasing values of Schmidt number, Brownian motion parameter, whereas the reverse effect is observed in the case of thermophoresis parameter, Soret number, and mass Biot number.

Table 5 Rate of mass transfer coefficient results

Nt	*Nb*	*Sc*	*Sr*	*ζ*	Sh_x
0.3	0.5	0.22	0.5	0.5	1.1267648934
0.6					1.1516570250
0.9					1.1767643709
	1.0				1.1447783135
	1.5				1.1615673058
		0.30			1.0875690465
		0.78			1.0516496981
			1.0		1.1446734992
			1.5		1.1616843924
				1.0	1.1336574023
				1.5	1.1516474391

- Incipiently, the present numerical results are in veritably good agreement with the published results of Nadeem et al. (35) in some special cases.

Scope for future research work

The finite element method employed in the current study can be used in future research since it is a highly useful approach to solving linear and nonlinear partial and ordinary differential equations in physics, mechanical engineering, and other related subjects. The resulting findings are more accurate than those obtained using other numerical approaches. Mechanical engineers currently employ the FEM to solve complex problems.

Abbreviations

u, v, w	Velocity components in *x*, *y*, and *z* axes, respectively (*m/s*)
x, y, z	Cartesian coordinates measured along the stretching sheet (*m*)
f	Dimensionless stream function along *x*-direction (*kg/m. s*)
f′	Fluid velocity along *x*-direction(*m/s*)
g	Dimensionless stream function along *y*-direction (*kg/m. s*)
g′	Fluid velocity along *y*-direction(*m/s*)
Pr	Prandtl number
T	Fluid temperature (*K*)
V_o	Constant velocity
T_f	Temperature of hot fluid (*K*)
T_∞	Temperature of the fluid far away from the stretching sheet (*K*)
Cf_x	Skin-friction coefficient along *x*-direction (s^{-1})
M	Magnetic field parameter
B_o	Uniform magnetic field (*Tesla*)
Cf_y	Skin-friction coefficient along *y*-direction (s^{-1})
$u_w(x)$	Stretching velocity of the fluid along *x*-direction (*m/s*)
$v_w(y)$	Stretching velocity of the fluid along *y*-direction (*m/s*)
q_w	Heat flux coefficient
q_m	Mass flux coefficient
Nt	Thermophoresis parameter
Nb	Brownian motion parameter
k^*	Permeability of porous medium
Nu_x	Rate of heat transfer coefficient (or) Nusselt number
Sh_x	Rate of mass transfer coefficient (or) Sherwood number
C_p	Specific heat capacity of nano particles (*J/kg/K*)
C	Stretching sheet parameter
Re_x	Reynolds number along *x*-direction
Re_y	Reynolds number along *y*-direction
D_B	Brownian diffusion coefficient (m^2/s)

K Permeability parameter (m^{-1})
D_T Thermophoresis diffusion coefficient
Sr Soret number
C^* Material constant
Du Dufour number
C Fluid nanoparticle volume concentration (mol/m^3)
C_∞ Dimensional ambient volume fraction (mol/m^3)
C_s Concentration susceptibility
K_T Thermal diffusion ratio
D_m Solutal diffusivity of the medium
T_m Fluid mean temperature
U_o Constant velocity
L Reference length
C_f Dimensional concentration of hot fluid (mol/m^3)

Greek symbols
η Dimensionless similarity variable (m)
θ Dimensionless temperature (K)
v Kinematic viscosity (m^2/s)
σ Electrical Conductivity
ρ Fluid density (kg/m^3)
K Thermal conductivity of the fluid
τ_{wx} Wall shear stress along x-direction
τ_{wy} Wall shear stress along y-direction
φ Dimensionless nano-fluid concentration (mol/m^3)
δ Thermal Biot number
ζ Mass Biot number
β_1 Non-uniform heat transfer coefficient
λ_1 Non-uniform mass transfer coefficient
β Powell-Eyring fluid parameter
λ Powell-Eyring fluid parameter
a_m Thermal diffusivity (m^2/s)
χ Material constant
ϑ Velocity ratio parameter

Superscript
$'$ Differentiation w.r.t η

Subscripts
f Fluid
w Condition on the sheet
∞ Ambient conditions

Acknowledgements
Department of Applied Mathematics, Andhra University, Visakhapatnam and Department of Mathematics, Geethanjali College of Engineering and Technology, Cheeryal, India.

Authors' contributions
All authors have read and approved the manuscript.

Funding
No funding was obtained for this study.

Availability of data and materials
The datasets used and or analyzed during the current study are available from the corresponding author on reasonable request and all data generated or analyzed during this study are included in this published article.

Declarations

Competing interests
The authors declare that they have no competing interests.

Received: 16 August 2023 Accepted: 18 December 2023
Published online: 03 January 2024

References
1. Kuznetsov AV, Nield DA (2010) Natural convective boundary-layer flow of a nanofluid past a vertical plate. Int J Therm Sci 49(2):243–247

2. Kuznetsov AV, Nield DA (2011) Soret and Dufour effects on heat and mass transfer in a porous medium saturated by a nanofluid. Int J Heat Mass Transf 54(1–3):487–494
3. Chamkha AJ, Al-Mudhaf AF (2011) Mixed convection from a vertical surface in a nanofluid with Soret and Dufour effects. Chem Eng Commun 198(5):641–655
4. Esfahani JA, Doostani A (2012) Natural convection heat transfer of a nanofluid in a vertical cylindrical annulus in the presence of Soret and Dufour effects. Int J Heat Mass Transf 55(4):1289–1299
5. Jafaryar M, Hatami M (2013) Analytical solution for Soret and Dufour effects on natural convection in a vertical porous cavity filled with a nanofluid. J Heat Transfer 135(4):041501
6. Mohebbi R, Hatami M, Rashidi MM (2014) Natural convection in a tilted cavity filled with a nanofluid considering Soret and Dufour effects. Int J Heat Mass Transf 78:599–609
7. Pal D, Mondal H (2016) Soret and Dufour effects on unsteady MHD free convection flow of a nanofluid past an inclined plate with radiation and heat source. Results Phys 6:1128–1137
8. Mahdy A, Chamkha AJ (2017) Dufour and Soret effects on natural convection in a nanofluid-filled enclosure with active walls. Heat Transfer-Asian Res 46(3):256–277
9. Rahimi-Gorji M, Hatami M (2019) Effects of Soret and Dufour on natural convection of a nanofluid in a porous cavity with sinusoidal temperature variations. J Therm Anal Calorim 137(1):191–204
10. Manca O, Nardini S (2020) A review on double-diffusive natural convection in nanofluids. Energies 13(1):65
11. Rashidi S, Lorenzini G (2012) Effects of Soret and Dufour on MHD natural convection in a square cavity filled with a nanofluid. Chem Eng Sci 68(1):372–382
12. Saffari H, Domairry G, Rashidi MM (2014) The effect of Soret and Dufour on natural convection of a nanofluid in a triangular enclosure with sinusoidal temperature distribution on the bottom wall. Powder Technol 261:138–148
13. Hajmohammad MH, Aminossadati SM (2013) Soret and Dufour effects on natural convection of a nanofluid in a porous cavity using LBM. Int J Heat Mass Transf 57(2):706–715
14. Jalilpour MS, Hosseinizadeh SF, Ghasemi B (2018) Analysis of Soret and Dufour effects on mixed convection heat transfer of Al_2O_3-water nanofluid in a lid-driven cavity. Int J Heat Mass Transf 116:643–655
15. Marafie A, Chamkha AJ, Al-Salem K (2018) Heat and mass transfer in nanofluid over a stretching sheet with Soret and Dufour effects. Int J Heat Mass Transf 126:829–838
16. Samet H, Abbasian Arani A (2017) Soret and Dufour effects on the flow and heat transfer of nanofluids over a stretching sheet with variable thickness. J Taiwan Inst Chem Eng 70:418–428
17. Kumar S, Singh AK (2018) Soret and Dufour effects on MHD flow of nanofluid over a vertical plate with convective boundary condition. Alex Eng J 57(3):1803–1813
18. Javed T, Hussain A, Hayat T, Alsaedi A (2018) Three-dimensional flow of Powell-Erying nanofluid with Soret and Dufour effects: a numerical study. Result Phys 10:859–865
19. Khan MI, Hayat T, Alsaedi A (2018) Simulation of double diffusion effects on Powell-Erying nanofluid with heat generation/absorption. J Therm Anal Calorim 133(1):31–43
20. Makinde OD, Motsa SS, Sibanda P (2018) Unsteady MHD flow of Powell-Erying nanofluid with Soret and Dufour effects. Results Phys 11:698–707
21. Motsa SS, Makinde OD, Sibanda P (2019) Soret and Dufour effects on MHD Powell-Eyring fluid flow over a convectively heated stretching sheet. J Appl Fluid Mech 12(4):1119–1126
22. Bég OA, Rashidi MM (2016) Soret and Dufour effects on the peristaltic transport of a Powell-Eyring fluid in an asymmetric channel. J Mol Liq 215:633–645
23. Das K, Sahoo B (2017) Soret and Dufour effects on MHD Powell-Eyring fluid flow past a stretching sheet. J Braz Soc Mech Sci Eng 39(10):4197–4211
24. Mustafa M, Hayat T, Alsaedi A (2016) Soret and Dufour effects on magnetohydrodynamic Powell-Eyring fluid flow with heat transfer. J Magn Magn Mater 401:44–55
25. Sulochana C, Vijaya Kumar PV (2018) Influence of Soret and Dufour effects on heat and mass transfer of Powell-Eyring fluid past a stretching sheet. Ain Shams Eng J 9(3):633–643
26. Alam MS, Ferdows M, Saha SC (2020) Soret and Dufour effects on unsteady Powell-Eyring fluid flow over a stretching sheet. J Braz Soc Mech Sci Eng 42(6):1–14
27. Partha MK, Nandy SK, Haldar SC (2021) MHD Powell-Eyring fluid flow over a stretching sheet with Soret and Dufour effects. J Magn Magn Mater 531:168860
28. Hayat T, Qasim M, Shehzad SA, Alsaedi A, Alhothuali MS (2016) MHD flow of Powell-Eyring fluid with thermal radiation and chemical reaction. J Mol Liq 223:555–562
29. Ramzan M, Ellahi R, Khan MI, Murtaza A (2019) Non-linear heat and mass transfer with Soret and Dufour effects in Powell-Eyring fluid over a stretching sheet. J Mol Liq 273:8–16
30. Khalid A, Shahzad A, Hayat T, Alsaedi A (2019) Effects of thermal radiation and convective condition on the Powell-Eyring fluid model with Dufour and Soret effects. Results in Physics 15:102612
31. Khan MI, Ullah I, Ellahi R (2019) Non-linear radiative flow of Powell-Eyring fluid over a stretching cylinder with Soret and Dufour effects. J Mol Liq 285:654–662
32. Khan MI, Ullah I, Ellahi R (2020) Numerical analysis of Powell-Eyring fluid over a nonlinear stretching sheet with Soret and Dufour effects. J Mol Liq 303:112657
33. Raja MAZ, Hussain A, Ali N, Ayub M (2020) Numerical investigation of Powell-Eyring fluid flow with Dufour and Soret effects. J Mol Liq 309:113037
34. Saqib M, Alsaedi A (2021) Soret and Dufour effects on the heat and mass transfer in a Powell-Eyring fluid model over a stretching surface. J Mol Liq 336:116383
35. Gundagani M, Sheri S, Paul A, Reddy MCK (2013) Radiation effects on an unsteady MHD convective flow past a semi-infinite vertical permeable moving plate embedded in a porous medium with viscous dissipation. Walailak J Sci Tech 10(5):499–515
36. Deepa Gadipally, Murali Gundagani (2014) Analysis of soret and dufour effects on unsteady MHD flow past a semi infinite vertical porous plate via finite difference method, Int J Appl Phys Math 4(5):332–344. https://doi.org/10.7763/IJAPM.2014.V4.306,2014

37. M Gundagani, MCK Reddy, S. Sivaiah (2012) Finite element solution of thermal radiation effect on unsteady MHD flow past a vertical porous plate with variable suction. Am Acad Scholarly Res J 4(3):3–22
38. Murali G, Paul A, Babu NVN (2015) Heat and mass transfer effects on an unsteady hydromagnetic free convective flow over an infinite vertical plate embedded in a porous medium with heat absorption. Int J Open Problems Compt Math 8(1):2015
39. Babu NVN, Paul A, Murali G (2015) Soret and Dufour effects on unsteady hydromagnetic free convective fluid flow past an infinite vertical porous plate in the presence of chemical reaction. J Sci Arts 15(1):99–111
40. Nadeem S, Haq RU, Akbar NS, Khan ZH (2013) MHD three-dimensional Casson fluid flow past a porous linearly stretching sheet. Alexandria Eng J 52(2013):577–582

Publisher's Note